nature climate change

LETTERS

PUBLISHED ONLINE: 5 OCTOBER 2014 | DOI: 10.1038/NCLIMATE2389

Quantifying underestimates of long-term upper-ocean warming

Paul J. Durack[1]*, Peter J. Gleckler[1], Felix W. Landerer[2] and Karl E. Taylor[1]

The global ocean stores more than 90% of the heat associated with observed greenhouse-gas-attributed global warming[1–4]. Using satellite altimetry observations and a large suite of climate models, we conclude that observed estimates of 0–700 dbar global ocean warming since 1970 are likely biased low. This underestimation is attributed to poor sampling of the Southern Hemisphere, and limitations of the analysis methods that conservatively estimate temperature changes in data-sparse regions[5–7]. We find that the partitioning of northern and southern hemispheric simulated sea surface height changes are consistent with precise altimeter observations, whereas the hemispheric partitioning of simulated upper-ocean warming is inconsistent with observed *in-situ*-based ocean heat content estimates. Relying on the close correspondence between hemispheric-scale ocean heat content and steric changes, we adjust the poorly constrained Southern Hemisphere observed warming estimates so that hemispheric ratios are consistent with the broad range of modelled results. These adjustments yield large increases (2.2–7.1 × 10^{22} J 35 yr^{-1}) to current global upper-ocean heat content change estimates, and have important implications for sea level, the planetary energy budget and climate sensitivity assessments.

Numerous studies have examined the long-term (~1950-present) global average and basin-scale evolution of ocean heat content (OHC) change in the upper 0–700 dbar (refs 1,4,8–12) (Supplementary Information) and important advancements have been made to correct for systematic measurement biases[6,13,14]. Evidence exists for a poleward shift of the subtropical gyres and marked warming in the Southern Ocean[7,15–17], but limitations of methods used to 'infill' these data-sparse regions may introduce a conservative bias toward low magnitude (zero) changes[5–7]. Recent estimates of OHC change attempt to address sampling deficiencies by relying on coincident sea surface height (SSH) estimates or the modern Argo array[8,9,12,18]. Additional ocean warming studies apply formal detection and attribution approaches that rely on intrinsic variability estimates from models, and avoid using infilled data by 'subsampling' models in space and time, consistent with the sparse historical observations[19–22].

Here, we investigate the large-scale spatial structure of OHC changes in five observational estimates (derived independently with differing processing choices) that were evaluated in the IPCC Fifth Assessment Report[4]. Based on a series of consistency checks with precise altimetry data and a large ensemble of climate models (Coupled Model Intercomparison Project (CMIP) phases 3 and 5), we find that observed Southern Hemisphere (SH) 0–700 dbar OHC changes are significantly underestimated. We analyse the 35-year period (1970–2004) over which both the CMIP5 'historical' data are available and during which observational sampling deficiencies are small enough to yield reliable OHC changes, at least in the Northern Hemisphere (NH; ref. 21).

OHC changes from the surface to 700 dbar are first examined in four observational estimates for which infilled gridded data were available[10,11,18,23] (Supplementary Fig. 2a and Methods); a fifth data set (Dom08; ref. 8) provides only hemispheric time series, but is included in subsequent analyses below. In Fig. 1a we show one of the observed results (Lev12; ref. 11) alongside the CMIP5 historical multi-model mean (MMM, Fig. 1b). To facilitate comparison of the observed and simulated spatial structure of OHC changes, additional maps show results with the global average removed (Fig. 1c,d and Supplementary Fig. 2a: A2–E2). The regions of inconsistency among the data sets are stippled, indicating where at least one of the four observational estimates disagrees in the sign of the mapped change (Fig. 1a,c and Supplementary Fig. 2a: A1–D1, A2–D2), or where fewer than 75% of models agree with the MMM sign (Fig. 1b,d and Supplementary Fig. 2a: E1, E2 and Fig. 2b: A2–D2, E2–I2). A prominent SH warming feature (30° S–50° S) is evident in MMM trend maps (Fig. 1b,d and Supplementary Fig. 2b), consistent with previous modelling studies[24,25]. This strong warming is less distinct in all observational analyses (Supplementary Fig. 2a), which is likely due to SH data sparsity and internal variability that can mask the externally forced warming in this region. As expected, the MMM is smoother than the observed analyses because uncorrelated variability present in individual simulated records is averaged out (Supplementary Fig. 2a: A2–D2).

Oceanographic theory[26] and models[24,25] (Fig. 1d and Supplementary Fig. 2b) suggest that shallow (above 700 dbar) ocean ventilation sites in the Southern Ocean (30° S–60° S) and the North Atlantic will warm at a faster rate than the global average ocean. These patterns are broadly compatible with ocean ventilation proxies, diagnosed from anthropogenic CFC-11 tracer concentrations in the observed ocean, and are well replicated by a smaller CMIP5 model subset (Supplementary Fig. 3 and Supplementary Information).

Observational estimates of OHC are not completely independent as they share data sources and in some cases apply similar processing procedures. The Ish09 (ref. 10) and Lev12 (ref. 11; Supplementary Fig. 2a: B1,B2 and C1,C2) data sets rely on similar objective analysis methods and data sources (including XBTs, which require non-trivial bias corrections), and both show a weak SH warming (compared to the NH), but a strong North Atlantic warming. These features are also present, although smaller in magnitude, in the Smi07 (ref. 23) result (Supplementary Fig. 2a: A1,A2), which uses the covariance field obtained from the HadCM3 model

[1]Program for Climate Model Diagnosis and Intercomparison, Lawrence Livermore National Laboratory, Livermore, California 94550, USA, [2]Jet Propulsion Laboratory, California Institute of Technology, Pasadena, California 91109, USA. *e-mail: pauldurack@llnl.gov

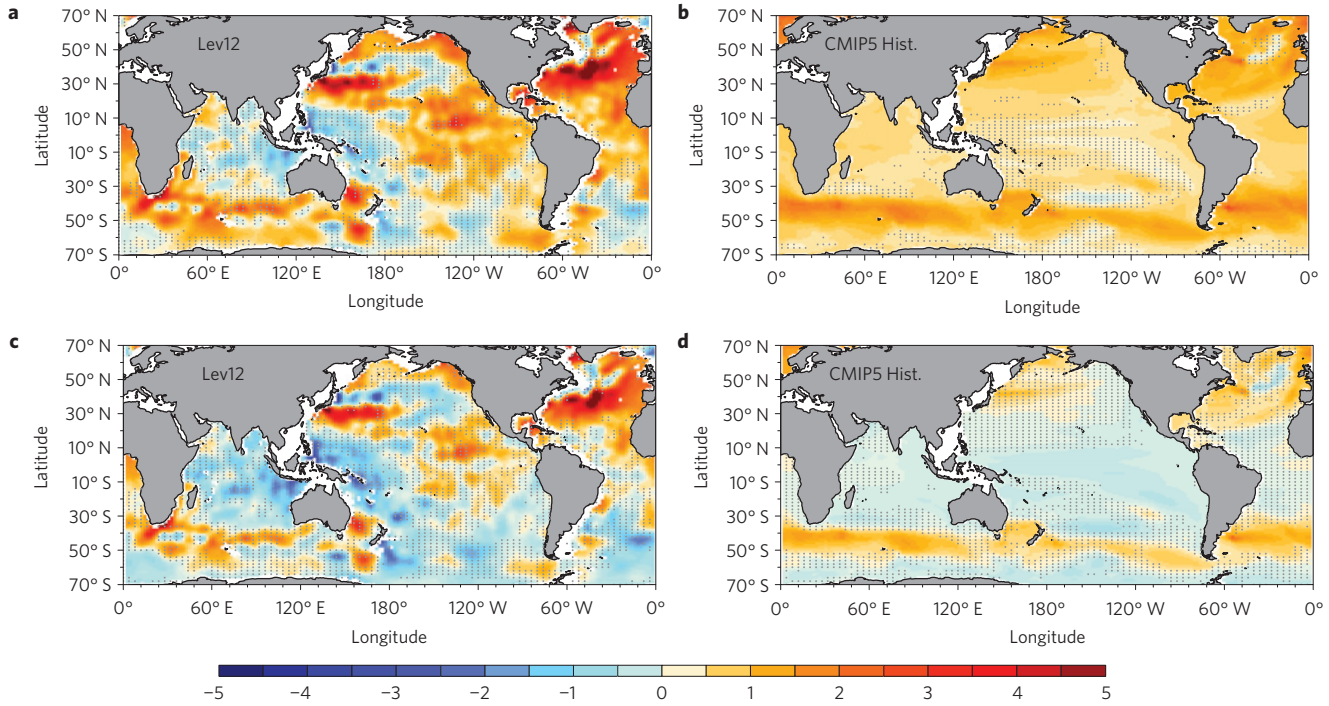

Figure 1 | Upper-ocean (0–700 dbar) heat content trends for 1970–2004. a,**c**, Observations taken from Lev12 (ref. 11). **b**,**d**, MMM results taken from CMIP5 historical simulations. Lower panels (**c**,**d**) show maps with the global average trends removed. All trends are reported in units of J $\times 10^3$ kg^{-1} 35 yr^{-1} (a value of 4 being approximately equivalent to 1 °C 35 yr^{-1} depth-averaged warming). Stippling marks regions where the four observational estimates do not agree in sign (**a**,**c**) or where >25% of the models simulate trends with a sign opposite to the MMM (**b**,**d**). Maps for the alternative observational estimates and for several additional CMIP experiments are shown in Supplementary Fig. 2a,b respectively.

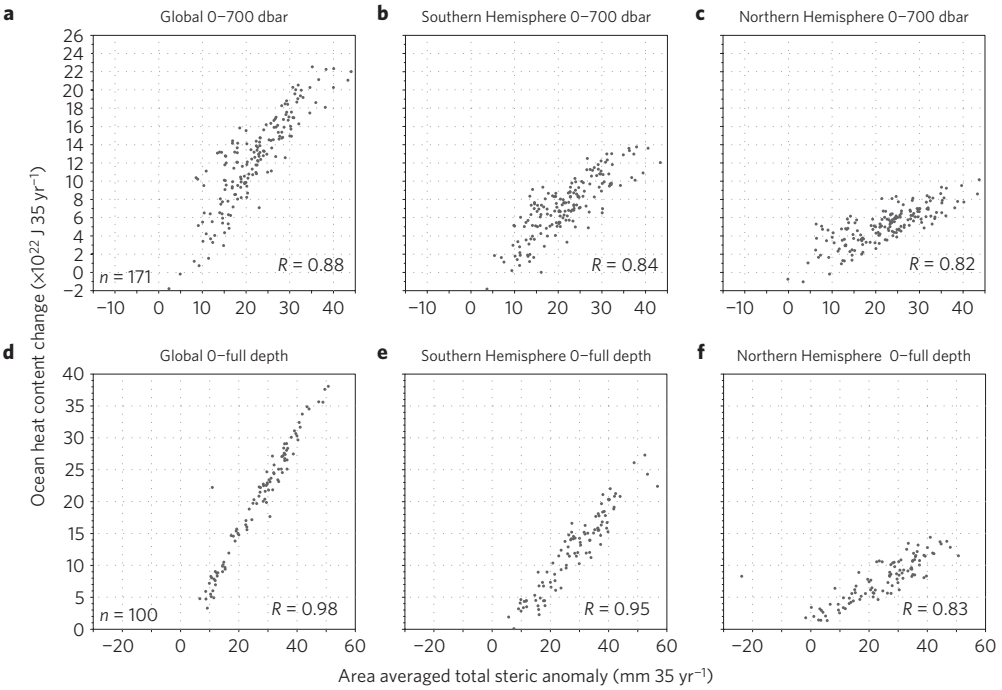

Figure 2 | Global and hemispheric OHC compared to total steric anomalies simulated by models for 1970–2004. The CMIP5 historical volume-integrated 35-year trends in OHC change are plotted against area-weighted average total steric anomalies (equivalent to SSH) for the upper 700 dbar in the upper panels (**a**–**c**) and for the full-depth ocean in the lower panels (**d**–**f**). The full-depth ocean analysis requires drift correction—consequently, fewer models were assessed.

to infill gaps in data-sparse areas (Supplementary Information). The DW10 (ref. 18) analysis, which is based on a smaller data set of more accurate hydrographic measurements (excluding XBTs), suggests a more homogeneous warming, with larger magnitudes in the South Pacific and South Atlantic basins compared to the other analyses (Supplementary Fig. 2a: D1,D2). In each of the four

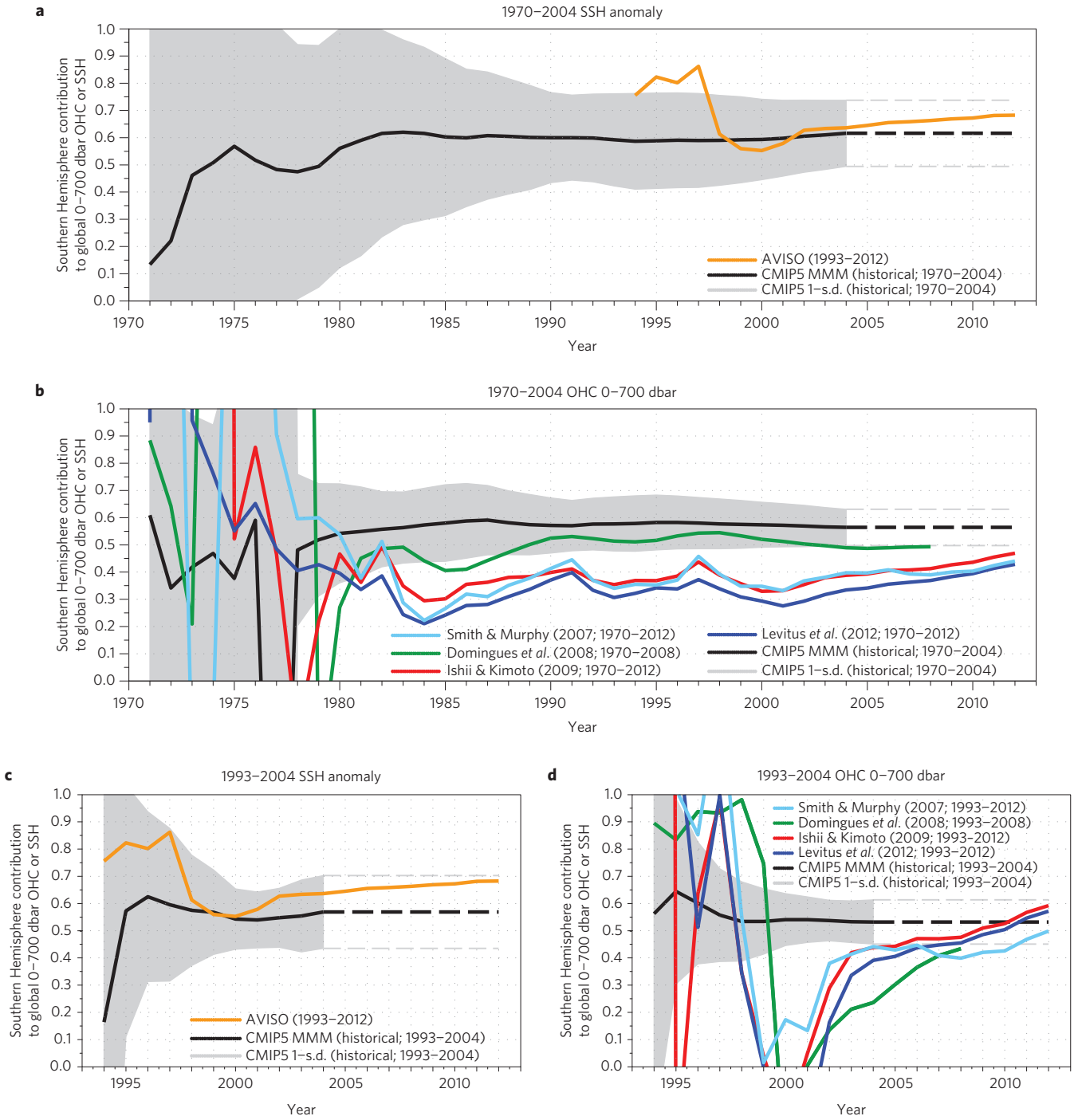

Figure 3 | Southern Hemisphere fractional contributions to global upper-OHC or global average SSH anomaly for varying trend lengths (1–35 years). **a**,**b**, Results over 1–35-years (1970–2004) for SSH (**a**) and OHC (**b**). **c**,**d**, Results for a shorter 11-year period (1993–2004) for SSH (**c**) and OHC (**d**) during which observed SSH data is available. Observed results extend to 2012 if available. Discontinuous black and grey lines extend 2004 CMIP5 values to 2012. The CMIP5 MMM and one standard deviation spread are obtained from CMIP5 historical simulations.

observed analyses, the Atlantic basin is warming at a faster rate than the Pacific, with the largest values found in the well-sampled North Atlantic, a feature also apparent in the CMIP ensembles (Fig. 1b,d and Supplementary Fig. 2b).

Although internal variability could explain a large portion of the discrepancy between the observed and modelled estimates of OHC change (Supplementary Information), contributions from systematic model or observational errors are also possible. To investigate the influence of such biases, and to test the physical consistency of model simulations, we compare simulated changes in SSH to satellite altimetry measurements (Supplementary Information). SSH reflects ocean changes driven by steric expansion as the oceans warm (accounting for approximately 40% of the long-term average SSH change[27]), along with mass contributions from the cryosphere, halosteric effects from regional salinity changes, and dynamic adjustments related to circulation changes. In models where glacial melt waters are not represented, SSH changes on hemispheric scales are almost entirely determined by full-depth steric changes, which are dominated by the thermal component and therefore closely related to OHC changes

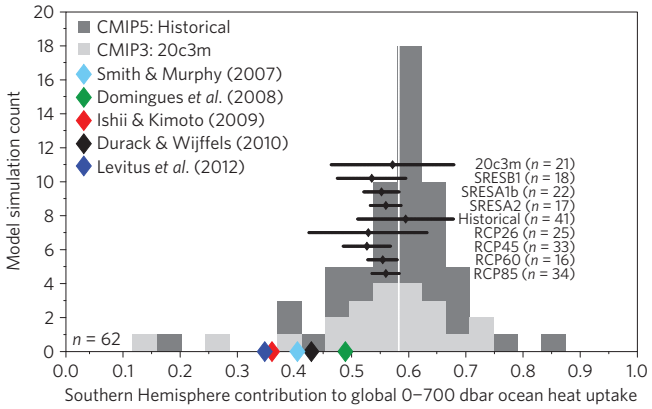

Figure 4 | Histogram of the observed and simulated Southern Hemisphere contribution to global OHC trends for 1970–2004. The distribution from 62 independent CMIP5 (historical) and CMIP3 (20c3m) model means (average of single model simulations) is shown in dark grey (21 CMIP3 20c3m simulations; overlaid light grey). Results from additional CMIP experiments are summarized with the MMM and one standard deviation spread indicated by small black diamonds and horizontal black lines respectively. The full ensemble MMM (dark grey) is presented as a vertical white line. Supplementary Fig. 8 shows composite single simulation distributions and Supplementary Fig. 9 shows each CMIP experiment. Models are listed in Supplementary Tables 1 and 2.

(Fig. 2 and Supplementary Fig. 4). Although the correspondence between simulated global average SSH and OHC is larger when the full ocean depth is considered (Fig. 2d), the strong correlation persists for the more variable upper-ocean (0–700 dbar; Fig. 2a). The close correspondence between OHC and SSH changes also holds at hemispheric scales (Fig. 2b,c and e,f) indicating that the better observed steric anomalies can be used as a proxy for the hemispheric partitioning of OHC change. A number of studies have relied on this relationship, and have used observed SSH to inform infilling approaches for the sparse temperature observations[8,28] or estimate sampling uncertainties[9,12] (Supplementary Information). The key benefit of SSH data is that, contrary to poorly sampled *in-situ* temperature, satellite altimetry data cover most of the globe and are sufficiently accurate to monitor changes since 1992.

We now contrast changes between the NH and SH by examining ratios of SH versus global changes for both OHC and SSH (Methods). This approach allows us to effectively calibrate *in-situ* temperature results between the relatively well sampled NH and poorly sampled SH.

We compare hemispheric ratios of SSH to their OHC counterparts considering linear trends over successively longer timescales. For the observed and simulated OHC changes we begin trend calculations in 1970, whereas for the observed SSH data we begin in 1993 (Fig. 3a,b). As expected, hemispheric trend ratios are noisy on decadal or shorter timescales owing to significant interannual variability; however, by 1990 (20-year trends) they have largely converged (Fig. 3a,b).

We also perform a similar analysis for the truncated time period (1993-present; Fig. 3c,d). Independent of the starting date, the observed SSH estimate lies well within the range of inter-model ratios for the CMIP5 historical simulations (0.68; Fig. 3a MMM 0.62 versus inter-model standard deviation 0.50–0.73; Fig. 3c MMM 0.57 versus 0.45–0.69). In contrast, the trends in the observed OHC ratio seem to be substantially smaller than simulated by most models, although they converge in recent years. The consistency between the observed and simulated SSH ratios suggests that the observed OHC discrepancy arises from SH sampling errors rather than from model biases.

All but one of the four observational OHC trend estimates in Fig. 3b suggest a much smaller SH contribution, with stabilized ratios at timescales of 15 years and longer, well outside the inter-model standard deviation (0.50–0.63, MMM 0.56 versus 0.33–0.49 for observations). With a 1993 start date (Fig. 3d), the OHC MMM trends stabilize within ten years, whereas the observational OHC ratios become progressively larger and trend toward better agreement with the modelled estimates (MMM 0.53 and inter-model standard deviation 0.45–0.61 Fig. 3d). This shift in the observed OHC trend is consistent with an increasing influence of Argo data after 2004, at which point *in-situ* measurements begin to provide near-global coverage[29]. Therefore, observational trend ratios become more consistent with the models as the SH data coverage improves and there is less need to infill. This result is evident when comparing the longer (1970–2012) versus the shorter (1993–2012) analysis period (Fig. 3b versus d).

To summarize, the following tests build our confidence in the range of simulated hemispheric ratios of OHC changes: hemispheric SSH 20-year trend ratios are consistent between altimetry observations and CMIP simulations (Fig. 3a,c); the relationship between SSH and OHC is strong and robust for the spatial scales considered (Fig. 2); and there is consistency between observed estimates and CMIP simulations for the vertical partitioning of OHC change in the upper (0–700 dbar) and full depth[4,30] (Fig. 2 and Supplementary Fig. 4). We note that there is probably a small positive SH contribution to observed SSH trends from a salinity(freshening)-driven halosteric expansion[18], which may account for some of the discrepancy between SSH and OHC ratios; however, this has little impact on our results.

We can further compare observed OHC ratios by analysing not only CMIP5 but also CMIP3 simulations. According to models, the OHC increases are about the same in both hemispheres. Thus, across all model simulations the average ratio of SH to global OHC change (0.59; Fig. 4) is close to the fraction of the global ocean volume for the SH (0.60). The observed ratios are smaller (0.35–0.49; Fig. 4), with the observational ratios largely inconsistent even when compared to each model experiment mean in isolation (Fig. 4, small black diamonds 0.52–0.58), or to a much larger composite distribution obtained from all available model simulations (633) across nine CMIP experiments (Supplementary Fig. 8, light grey). The resolved model-based hemispheric ratio is insensitive to forcing changes, as evidenced by comparing the 20c3m/historical results to the strongly forced projections (for example, SRESA2 and RCP85) that result in enhanced ocean stratification, mixed layer shoaling and changes to ocean ventilation rates (Supplementary Information).

Thus, it seems that our preliminary finding is robust: the SH contribution to the total upper-OHC change found in the five observational data sets is inconsistent with the CMIP model ensembles (Figs 3b and 4). The agreement between the observed and simulated SSH changes, the close correspondence between OHC and SSH (Fig. 2), and the better agreement of observed and simulated OHC for the recent Argo period (with improved SH coverage) suggests systematic model biases are not the dominant factor. We thus conclude, in agreement with previous works[5–7], that long-term observational estimates of SH upper-ocean heat content change are biased low.

If models are correct in their hemispheric partitioning of OHC changes, we can use them to guide observational adjustment over the data-sparse SH. Assuming that the much better sampled and more consistent estimates of observed NH OHC change (Supplementary Fig. 2a) are accurate, we adjust the poorly constrained SH estimates (Methods) so that they yield an inter-hemispheric ratio that is consistent with the MMM (Fig. 4). When this adjustment is applied, the various observational estimates of 35-year global upper-OHC change are substantially increased in all

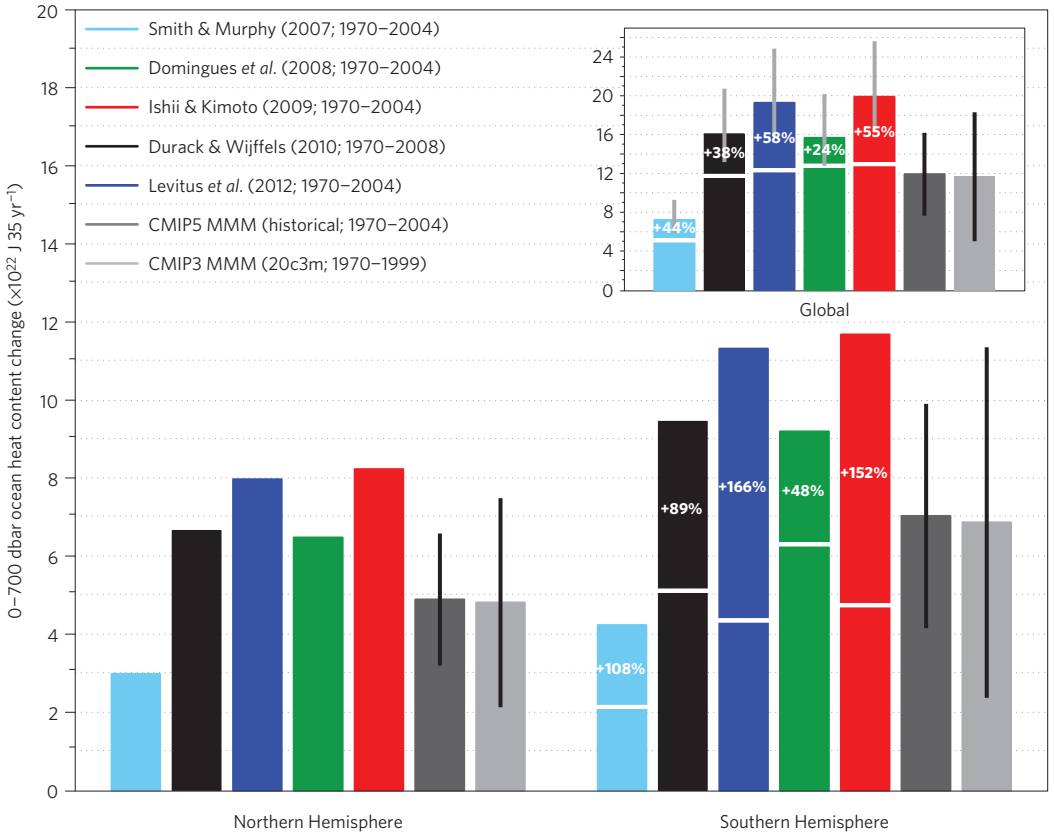

Figure 5 | Observed and simulated hemispheric and global upper-ocean (0–700 dbar) heat content change for 1970–2004. For the SH and global results horizontal white lines indicate the original unadjusted changes. Full bars indicate the adjusted values, which are revised so that hemispheric ratios of heat uptake match the MMM results from CMIP5 historical and CMIP3 20c3m simulations (Fig. 4). The NH and adjusted SH estimates are summed to yield global estimates (upper inset). Uncertainty estimates show the range of adjusted values obtained using the one standard deviation spread of model-simulated ratios (Fig. 4) and are indicated by vertical grey lines. Black vertical lines indicate the one standard deviation spread in simulated estimates for CMIP5 and CMIP3. All estimates represent 35-year changes, the period of the trend calculation is specified in parentheses in the legend.

cases. The adjusted estimates span the range from 7.2 to 19.9×10^{22} J (Fig. 5 upper inset; observed ratios 0.35–0.49 adjusted to 0.59; Fig. 4) and, depending on the observational analysis considered, correspond to increases of 48–166% for the SH and 24–58% for the global OHC (Fig. 5). To provide perspective, for each observational estimate we reapply our adjustment method using the modelled ratio obtained from the distribution of simulations (Fig. 4), and use a spread of one standard deviation to construct uncertainty bounds (Fig. 5 upper inset; grey lines). We note that the largest adjusted global values (Ish09 (ref. 10), Lev12 (ref. 11)) are consistent with a recent upper-OHC change estimate[12]; if uncertainty bounds are considered this agreement includes four of the five adjusted values (Fig. 5 upper inset).

We further investigate the consistency between observations and models by considering the warming for each hemisphere separately (Fig. 5, lower left and right bars). We consider results from CMIP3 and CMIP5 separately (Fig. 5 light and dark grey bars), and show the one standard deviation spread (black lines) between available CMIP5 historical (dark grey bars) and CMIP3 20c3m (light grey bars) simulations. Using this measure, only two of the five observations (Dom08 (ref. 8), DW10 (ref. 18)) seem consistent with the modelled range for both hemispheres. All but one observed estimate (Smi07 (ref. 23)) suggest a larger NH warming than the MMM values (Fig. 5; left bars), and all five observed estimates show a smaller SH warming than the MMM values (Fig. 5; right bars). The simulated NH changes are consistent with some, but not all of the better sampled NH observations, indicating that we cannot rule out an influence of model error on our adjustments.

Accurate estimates of global ocean warming are required to understand contributions to observed sea-level and energy budget changes and to constrain empirical estimates of climate sensitivity. Our analysis finds that modelled hemispheric ratios of SSH changes are consistent with highly accurate altimetry observations but remarkably inconsistent with *in-situ*-based hemispheric ratios of OHC changes. Adjusting the poorly constrained SH OHC change estimates to yield an improved consistency with models, produces a previously unaccounted for increase in global upper-OHC of $2.2–7.1\times10^{22}$ J above existing estimates for 1970 to 2004 (Fig. 5, upper inset). For perspective, these adjustments represent more than double the 1970–2004 heat storage change for all non-ocean (terrestrial, cryospheric and atmospheric) heat reservoirs combined[4], and highlights the importance of accurately estimating ocean temperature changes. By contrasting hemispheric changes in an attempt to quantify the impact of SH observation deficiencies, our analysis should motivate further work to improve estimates of global OHC change.

Methods

We constructed near-global, interpolated maps of annual average upper-OHC along with hemispheric time series for CMIP5 historical (1970–2004), CMIP3 20c3m (1970–1999) and CMIP3/5 future model simulations (2065–2099), as well as for five available observations (1970-near present: Smi07 (ref. 23), Dom08 (ref. 8), Ish09 (ref. 10), DW10 (ref. 18) and Lev12 (ref. 11)).

The hemispheric time series were computed with equal-area weighting from native model and observational grids and native land–sea masks, which in most cases extend from 90° S to 90° N (Fig. 3).

The mapped data is interpolated to a regular horizontal (70° S–70° N) and vertical (0–700 dbar) grid for all models and observations, using an identical

land–sea mask which excludes marginal seas, the Arctic Ocean and the high-latitude Southern Ocean (Fig. 1 and Supplementary Fig. 2a,b). After interpolation, an iterative nearest-neighbour infilling algorithm is employed to ensure the geographic coverage of each estimate is identical. We used a pre-computed and updated hemispheric time series from the Dom08 (refs 8,21) analysis, as a gridded analysis was not available.

We contrast observed and modelled SSH to assess the possible effect of model biases on our simulated OHC hemispheric totals. SSH is analysed to investigate the internal consistency between ocean warming and total steric change, and we show these quantities are highly correlated over the hemispheric scales considered (Fig. 2 and Supplementary Fig. 4). The hemispheric contribution to global average SSH changes in both observations and models show a strong agreement (Fig. 3a,c). This strong hemispheric SSH agreement provides the motivation to assess modelled hemispheric OHC and compare this to observed estimates.

We calculate the contribution to global upper-OHC change obtained from the SH alone, and contrast these ratios over the analysed period comparing the MMM for the CMIP5 historical and CMIP3 20c3m simulations (R; Fig. 4) and observations respectively. Guided by the observed and modelled consistency in SSH, we correct observations by scaling the observed SH/Global ratio to match the simulated ratio of the CMIP5/3 MMM (Fig. 4). This technique leverages the better-sampled observed NH oceans and the SH/Global OHC ratio obtained from the CMIP models to provide a correction term (x) for the poorly constrained SH OHC change estimate ($\mathrm{SH}_{\mathrm{Obs}}$). Once we have corrected the SH OHC change estimate, we then use this ($\mathrm{SH}^{*}_{\mathrm{Obs}}$) along with the existing NH OHC change estimate ($\mathrm{NH}_{\mathrm{Obs}}$) to recalculate the corrected global upper-OHC change total ($\mathrm{Global}^{*}_{\mathrm{Obs}}$) following equations (1)–(4) below:

$$R = \frac{\mathrm{SH}_{\mathrm{Models}}}{(\mathrm{SH}_{\mathrm{Models}} + \mathrm{NH}_{\mathrm{Models}})} = \frac{\mathrm{SH}_{\mathrm{Obs}} \times x}{((\mathrm{SH}_{\mathrm{Obs}} \times x) + \mathrm{NH}_{\mathrm{Obs}})} \quad (1)$$

$$x = \frac{R \times \mathrm{NH}_{\mathrm{Obs}}}{(1-R) \times \mathrm{SH}_{\mathrm{Obs}}} \quad (2)$$

$$\mathrm{SH}^{*}_{\mathrm{Obs}} = \mathrm{SH}_{\mathrm{Obs}} \times x \quad (3)$$

$$\mathrm{Global}^{*}_{\mathrm{Obs}} = \mathrm{SH}^{*}_{\mathrm{Obs}} + \mathrm{NH}_{\mathrm{Obs}} \quad (4)$$

To provide a measure of our correction uncertainty we use a one standard deviation spread of the SH/Global ratio from the available simulations (Fig. 4). These are used to generate representative uncertainty bars for our global upper-OHC estimates (Fig. 5; upper inset, grey bars). We note that this provides a simplified uncertainty estimate; however, owing to the large number of observational analyses and model simulations used in the study a more complex treatment was not undertaken.

To enhance the model ensemble sample size, CMIP3 20c3m (1970–1999) simulations and CMIP3 and CMIP5 future projections (2050–2099; SRES and RCPs) are also sampled to assess the potential role of forcing on hemispheric ratios.

Model drift was not explicitly corrected, as drift is primarily an issue in the deeper ocean (>2,000 dbar) and correction considerably reduced the number of available simulations. Instead, we calculated the impact of drift correction on a specific sub-suite of the CMIP5 historical simulations (Supplementary Figs 10 and 11). We found that for the drift-corrected models this changed the MMM ratios by a negligible amount (<2%); therefore, the hemispheric analysis was found to be insensitive to drift correction. The full-depth analysis which compares OHC change to total steric changes (Fig. 2d–f) required drift correction, which accounts for spurious deep-ocean anomalies, and owing to limited data availability reduced the number of available simulations from 171 to 100 (Fig. 2).

For more detailed descriptions and supporting figures please refer to the Supplementary Information.

Received 24 March 2014; accepted 29 August 2014; published online 5 October 2014

References

1. Levitus, S., Antonov, J. & Boyer, T. Warming of the world ocean, 1955–2003. *Geophys. Res. Lett.* **32,** L02604 (2005).
2. Church, J. A. *et al.* Revisiting the Earth's sea-level and energy budgets from 1961 to 2008. *Geophys. Res. Lett.* **38,** L18601 (2011).
3. Otto, A. *et al.* Energy budget constraints on climate response. *Nature Geosci.* **6,** 415–416 (2013).
4. Rhein, M. *et al.* in *Climate Change 2013: The Physical Science Basis* (eds Stocker, T. F. *et al.*) Ch. 3, 255–315 (IPCC, Cambridge Univ. Press, 2013).
5. Gregory, J. M., Banks, H. T., Stott, P. A., Lowe, J. A. & Palmer, M. D. Simulated and observed decadal variability in ocean heat content. *Geophys. Res. Lett.* **31,** L15312 (2004).
6. Gouretski, V. & Koltermann, K. P. How much is the ocean really warming? *Geophys. Res. Lett.* **34,** L01610 (2007).
7. Gille, S. T. Decadal-scale temperature trends in the southern hemisphere ocean. *J. Clim.* **21,** 4749–4765 (2008).
8. Domingues, C. M. *et al.* Improved estimates of upper-ocean warming and multi-decadal sea-level rise. *Nature* **453,** 1090–1093 (2008).
9. Lyman, J. M. & Johnson, G. C. Estimating annual global upper-ocean heat content anomalies despite irregular *in situ* ocean sampling*. *J. Clim.* **21,** 5629–5641 (2008).
10. Ishii, M. & Kimoto, M. Reevaluation of historical ocean heat content variations with time-varying XBT and MBT depth bias corrections. *J. Oceanogr.* **65,** 287–299 (2009).
11. Levitus, S. *et al.* World ocean heat content and thermosteric sea level change (0–2000 m), 1955–2010. *Geophys. Res. Lett.* **39,** L10603 (2012).
12. Lyman, J. M. & Johnson, G. C. Estimating global ocean heat content changes in the upper 1800 m since 1950 and the influence of climatology choice*. *J. Clim.* **27,** 1945–1957 (2014).
13. Wijffels, S. E. *et al.* Changing expendable bathythermograph fall rates and their impact on estimates of thermosteric sea level rise. *J. Clim.* **21,** 5657–5672 (2008).
14. Cowley, R., Wijffels, S., Cheng, L., Boyer, T. & Kizu, S. Biases in expendable bathythermograph data: A new view based on historical side-by-side comparisons. *J. Atmos. Ocean. Technol.* **30,** 1195–1225 (2013).
15. Gille, S. T. Warming of the southern ocean since the 1950s. *Science* **295,** 1275–1277 (2002).
16. Aoki, S., Bindoff, N. L. & Church, J. A. Interdecadal water mass changes in the southern ocean between 30° E and 160° E. *Geophys. Res. Lett.* **32,** L07607 (2005).
17. Alory, G., Wijffels, S. & Meyers, G. Observed temperature trends in the Indian Ocean over 1960–1999 and associated mechanisms. *Geophys. Res. Lett.* **34,** L02606 (2007).
18. Durack, P. J. & Wijffels, S. E. Fifty-year trends in global ocean salinities and their relationship to broad-scale warming. *J. Clim.* **23,** 4342–4362 (2010).
19. Barnett, T. P. *et al.* Penetration of human-induced warming into the world's oceans. *Science* **309,** 284–287 (2005).
20. AchutaRao, K. M. *et al.* Variability of ocean heat uptake: Reconciling observations and models. *J. Geophys. Res.* **111,** C05019 (2006).
21. Gleckler, P. J. *et al.* Human-induced global ocean warming on multidecadal timescales. *Nature Clim. Change* **2,** 524–529 (2012).
22. Pierce, D. W., Gleckler, P. J., Barnett, T. P., Santer, B. D. & Durack, P. J. The fingerprint of human-induced changes in the ocean's salinity and temperature fields. *Geophys. Res. Lett.* **39,** L21704 (2012).
23. Smith, D. M. & Murphy, J. M. An objective ocean temperature and salinity analysis using covariances from a global climate model. *J. Geophys. Res.* **112,** C02022 (2007).
24. Banks, H. T. & Gregory, J. M. Mechanisms of ocean heat uptake in a coupled climate model and the implications for tracer based predictions of ocean heat uptake. *Geophys. Res. Lett.* **33,** L07608 (2006).
25. Fyfe, J. C. Southern ocean warming due to human influence. *Geophys. Res. Lett.* **33,** L19701 (2006).
26. Talley, L. D. Shallow, intermediate, and deep overturning components of the global heat budget. *J. Phys. Oceanogr.* **33,** 530–560 (2003).
27. Church, J. A. *et al.* in *Climate Change 2013: The Physical Science Basis* (eds Stocker, T. F. *et al.*) Ch. 13, 1137–1216 (IPCC, Cambridge Univ. Press, 2013).
28. Church, J. A., White, N. J., Coleman, R., Lambeck, K. & Mitrovica, J. X. Estimates of the regional distribution of sea level rise over the 1950–2000 period. *J. Clim.* **17,** 2609–2625 (2004).
29. Roemmich, D. & Gilson, J. The 2004–2008 mean and annual cycle of temperature, salinity, and steric height in the global ocean from the Argo program. *Prog. Oceanogr.* **82,** 81–100 (2009).
30. Flato, G. *et al.* in *Climate Change 2013: The Physical Science Basis* (eds Stocker, T. F. *et al.*) Ch. 9, 741–866 (IPCC, Cambridge Univ. Press, 2013).

Acknowledgements

The work of P.J.D., P.J.G. and K.E.T. from Lawrence Livermore National Laboratory is a contribution to the US Department of Energy, Office of Science, Climate and Environmental Sciences Division, Regional and Global Climate Modeling Program under contract DE-AC52-07NA27344. The work of F.W.L. was performed at the Jet Propulsion Laboratory, California Institute of Technology and is supported by NASA ROSES Physical Oceanography grant NNN13D462T and the NASA Sea Level Change Team (NSLCT). We thank numerous colleagues from the Program for Climate Model Diagnosis and Intercomparison (PCMDI) for valuable feedback and input into this project. We also thank J. Durack of the University of California, San Francisco (USA), M. V. Durack of educAID (Australia), T. P. Boyer from the National Oceanographic Data Center, Silver

Spring (USA), C. M. Domingues from the Antarctic Climate and Ecosystems CRC, Hobart (Australia) and J. A. Church from the Centre for Australian Weather and Climate Research, Hobart (Australia). We acknowledge the sources of observed data used in this study: D. Smith and J. Murphy (Smi07), C. M. Domingues (Dom08), M. Ishii and M. Kimoto (Ish09), S. Levitus and T. Boyer (Lev12) and the International Argo Program and the national programs that contribute to it. We acknowledge the World Climate Research Programme's Working Group on Coupled Modelling, which is responsible for CMIP, and we thank the climate modelling groups (listed in Supplementary Tables 1 and 2) for producing and making available their model output. For CMIP the US Department of Energy's Program for Climate Model Diagnosis and Intercomparison provides coordinating support and led development of software infrastructure in partnership with the Global Organization for Earth System Science Portals. The DW10 data presented in this study can be downloaded from the CSIRO Ocean Change website at www.cmar.csiro.au/oceanchange. LLNL Release #: LLNL-JRNL-651841.

Author contributions

P.J.D. completed the OHC analysis, P.J.G. assisted in the OHC analysis and F.W.L. completed the SSH analysis. All authors assisted with interpretation and shared responsibility for writing the manuscript.

Additional information

Supplementary information is available in the online version of the paper. Reprints and permissions information is available online at www.nature.com/reprints. Correspondence and requests for materials should be addressed to P.J.D.

Competing financial interests

The authors declare no competing financial interests.